Monolithic Integration via a Universal Damage Enhanced Quantum-Well Intermixing Technique

Stewart D. McDougall, Olek P. Kowalski, Craig J. Hamilton, Fernando Camacho, Bocang Qiu, Maolong Ke, Richard M. De La Rue, *Senior Member, IEEE*, A. Catrina Bryce, *Member, IEEE*, and John H. Marsh, *Senior Member, IEEE*

(Invited Paper)

***Abstract*— A novel technique for quantum-well intermixing is demonstrated, which has proven a reliable means for obtaining postgrowth shifts in the band edge of a wide range of III–V material systems. The technique relies upon the generation of point defects via plasma induced damage during the deposition of sputtered SiO_2, and provides a simple and reliable process for the fabrication of both wavelength tuned lasers and monolithically integrated devices.**

Wavelength tuned broad area oxide stripe lasers are demonstrated in InGaAs–InAlGaAs, InGaAs-InGaAsP, and GaInP–AlGaInP quantum well systems, and it is shown that low absorption losses are obtained after intermixing. Oxide stripe lasers with integrated slab waveguides have also enabled the production of a narrow single lobed far field (3°) pattern in both InGaAs–InAlGaAs, and GaInP–AlGaInP devices. Extended cavity ridge waveguide lasers operating at 1.5 μm are demonstrated with low loss (α = 4.1 cm^{-1}) waveguides, and it is shown that this loss is limited only by free carrier absorption in waveguide cladding layers. In addition, the operation of intermixed multimode interference couplers is demonstrated, where four GaAs–AlGaAs laser amplifiers are monolithically integrated to produce high output powers of 180 mW in a single fundamental mode. The results illustrate that the technique can routinely be used to fabricate low-loss optical interconnects and offers a very promising route toward photonic integration.

***Index Terms*— Integrated optoelectronics, plasma materials-processing applications, quantum-well lasers, sputtering.**

I. Introduction

AN IMPORTANT goal for future optical communication systems is the development of optoelectronic integrated circuits, in which high bit rate information is transmitted between active devices through low-loss waveguides. Such integration would provide considerable advantages in terms of device miniaturization, resultant increases in component density and reductions in cost, improved reliability and robustness, simplified packaging and potential improvements in data handling rates. Quantum-well intermixing (QWI) techniques permit a postgrowth modification to the absorption edge of multiple-quantum-well (MQW) material, and therefore provide a flexible, reliable, simple and low-cost approach compared to competing integration schemes, such as selective area epitaxy, or selective etching and regrowth.

Since the initial demonstration of intermixing in the GaAs–AlGaAs system, a number of techniques have been developed including impurity induced disordering (IID) [1], impurity free vacancy disordering (IFVD) [2], various laser disordering processes [3]–[5] and ion implantation induced disordering [6]. IID techniques utilize surface dopant diffusion or ion implantation to introduce impurities within the crystal structure, the presence of which alters the Fermi level and enhances the solubility of certain point defects, resulting in an increased rate of atomic interdiffusion during a subsequent anneal stage [7]. The technique has been used to intermix GaAs–AlGaAs, InGaAs–InGaAsP, and InGaAs–InAlGaAs MQW structures with varying degrees of success. As the IID technique requires an annealing stage, particular problems are encountered for the InGaAs–InGaAsP MQW system, where the poor thermal stability of the material enables only limited differential shifts between intermixed and intermixing suppressed regions. IID can also have deleterious effects in terms of the electrical characteristics of integrated devices, and can lead to increases in free carrier absorption due to the introduction of dopants within the active region, resulting in increased modal propagation losses. An extremely successful technique employed primarily in the GaAs–AlGaAs system is IFVD, in which a high-temperature anneal induces the out-diffusion of Ga from the epilayer cap into a suitable dielectric cap (e.g., SiO_2), leading to an increase in the Ga vacancy concentration at the surface and an enhanced Ga-Al interdiffusion rate [2]. While certain caps enhance the out-diffusion, others suppress it. It is, therefore, possible to achieve spatially selective intermixing using photolithographic patterning of the appropriate capping layers. Both SrF_2 [8] and P:SiO_2 [9] have proved effective caps for suppressing the intermixing process, enabling the fabrication of extended cavity lasers with low passive section loss. The poor thermal stability of the InGaAs–InGaAsP system makes it difficult to suppress intermixing, leading to the generation of only small and unreliable differential shifts using IFVD. However this poor thermal stability has been used to great advantage in the photoabsorption-induced disordering (PAID) process, in which photons from a 1064-nm CW Nd:YAG laser are absorbed in the InGaAs–InGaAsP active region, with the

Manuscript received January 12, 1998; revised June 16, 1998. This work was supported by the U.K. Engineering and Physical Sciences Research Council and by the Ministry of Defence, U.K.

The authors are with the Department of Electronics and Electrical Engineering, University of Glasgow, Glasgow G12 8QQ, Scotland, U.K.

Publisher Item Identifier S 1077-260X(98)06798-7.

subsequent carrier cooling and nonradiative recombination thermally intermixing the MQW layers [5]. The process allows large differential bandgap shifts to be achieved, with the processed material exhibiting extremely high optical and electrical characteristics. Spatial selectivity can be achieved by using a gold mask to reflect the incident photons and thereby prevent intermixing in regions in which it is not required. However, due to the thermal nature of the process, diffusion of heat beneath the gold mask leads to a poor spatial resolution for the process (100–200 μm), which limits its applications for monolithic integration. The use of ion implantation to generate point defects through high-energy impact with the crystal matrix elements has been used widely in many III–V material systems (AlGaAs, InP, etc.). This involves the use of relatively high energy ion implants to considerable depths ($> \sim 1$ μm), usually with electrically inactive implant species e.g., P and As. Although successful, the requirement for specialised facilities for implantation make this technique relatively complicated and expensive.

The new intermixing technique described here, is based on point defect generation during the deposition of sputtered SiO_2 and has so far proved highly successful for all of the above mentioned material systems. In addition to its wide range of applicability, it is impurity free, low cost and involves relatively simple processing stages, with only photoresist required for inhibition of intermixing. Along with a description of the intermixing process, and the demonstration of active and passive/integrated devices in the above materials, we also present results for the visible wavelength GaInP–AlGaInP MQW system for which no impurity free spatially selective intermixing technique has previously been demonstrated.

The content of the rest of this paper is as follows: Section II provides a general description of the intermixing process, going on to present results obtained in the InGaAs–InGaAsP and InGaAs–InAlGaAs systems; Section III describes the characterization of wavelength tuned devices fabricated from these material systems; in Section IV the results of intermixing experiments in the GaInP–AlGaInP material system are presented along with the operation of extended cavity broad-area lasers with an associated narrowing in the output far-field pattern; Section V illustrates the applicability of the technique for the fabrication of low-loss waveguides, through the characterization of extended cavity ridge waveguide lasers fabricated in InGaAs–InGaAsP material; Section VI presents intermixing data obtained for the GaAs–AlGaAs system and demonstrates the operation of intermixed GaAs-based multimode interference couplers, enabling the monolithic integration of four laser amplifier sections with a single output waveguide; in the final section the results of the preceding sections are summarized and some conclusions presented.

II. The Intermixing Process

In this section, a detailed account of the intermixing technique is given, concentrating on results obtained for the InGaAs–InAlGaAs and InGaAs–InGaAsP QW material systems. For both systems the intermixing process has been investigated in standard MQW laser structures, comprising a

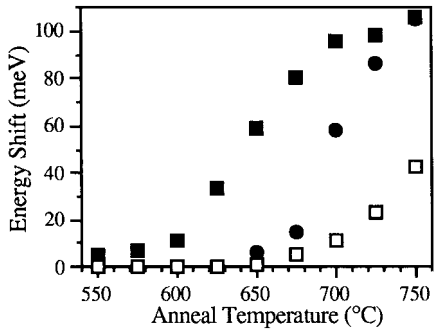

Fig. 1. Energy shift as a function of anneal temperature for InGaAsP capped with 200-nm sputtered (■) and PECVD (□) SiO_2, and InAlGaAs capped with 200-nm sputtered SiO_2 (•).

MQW active section, an undoped waveguide core, n- and p-type cladding layers and a highly doped p-type contact layer. Both structures were nominally lattice matched to an InP substrate. The InGaAsP structure was grown by metal organic vapor phase epitaxy (MOVPE) and comprised a MQW active section with 5×65 Å QW's separated by 120-Å InGaAsP ($\lambda = 1.26$ μm) barriers within a 0.36-μm-thick stepped graded index waveguide, surrounded by Si-doped n-type (1×10^{17} cm^{-3}) and Zn-doped p-type (1×10^{17} cm^{-3}) InP cladding layers with respective thicknesses of 1.0 and 1.4 μm. The sample was capped by a 100-nm-thick p^+ Zn-doped (1×10^{17} cm^{-3}) InGaAs layer. The InAlGaAs sample was grown by molecular beam epitaxy and comprised a 0.5-μm Si doped n-type InAlAs cladding layer (5×10^{17} cm^{-3}), a MQW active region containing 6×70 Å QW's separated by 80-Å InAlGaAs barriers centrally placed within a 0.34-μm undoped waveguide core, a 2-μm Be-doped (5×10^{17} cm^{-3}) p-type InAlAs cladding layer and a p^+ (1×10^{19} cm^{-3}) InGaAs cap.

The intermixing process described here simply involves the deposition of a thin layer of sputtered SiO_2 directly on to the semiconductor surface followed by a high temperature anneal (650 °C–750 °C) in a rapid thermal annealer (RTA). The sputtering was carried out in a Nordiko RF sputtering machine, using an Ar:O_2 gas mixture and an RF power of 100 W with a self dc bias of 1 kV and a gas pressure of 5×10^{-3} mbar. Following the sputtering and anneal stages, photoluminescence (PL) measurements performed at 77 K were used to determine the resultant bandgap shifts.

Fig. 1 shows the bandgap shifts obtained for InAlGaAs and InGaAsP samples capped with sputtered SiO_2 and SiO_2 deposited by plasma enhanced chemical vapor deposition (PECVD). For material capped with sputtered SiO_2 the intermixing rate is clearly enhanced, with bandgap shifts in the InGaAsP system occurring at temperatures as low as 550 °C, considerably below the intermixing threshold temperature in PECVD capped material, which occurs at 650 °C. The shifts under sputtered SiO_2 increase rapidly with annealing temperature up to over 70 meV at 650 °C. A similar enhancement is also observed for the InAlGaAs system, with material capped by sputtered SiO_2 undergoing bandgap shifts at temperatures as low as 600 °C and shifts in excess of 100 meV obtained at 750 °C. Meanwhile, over the same temperature range, InAlGaAs samples capped with PECVD SiO_2 exhibit no

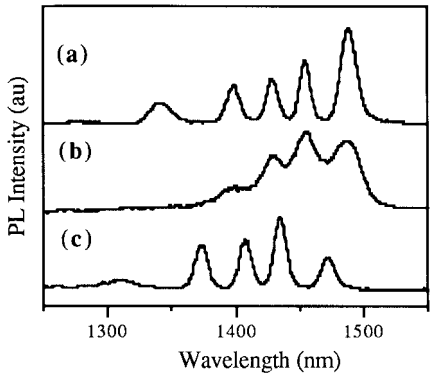

Fig. 2. (a) 4 K PL spectra obtained an InGaAsP MQW damage probe structure as-grown, (b) after deposition of sputtered SiO_2, and (c) after subsequent annealing at 500 °C.

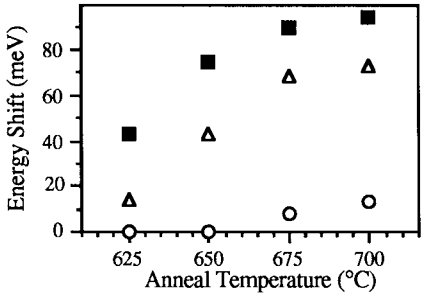

Fig. 3. Energy shift against anneal temperature, obtained following deposition of 200-nm sputtered SiO_2 for InGaAsP samples that are: uncapped (■), capped with 200-nm PECVD SiO_2 (△), and capped by an additional 1.8-μm photoresist layer (○).

measurable bandgap shift. This clearly illustrates the potential of the technique for producing large bandgap shifts while, at the same time, completely suppressing the bandgap shifts in regions in which intermixing is not required.

The intermixing mechanism has been investigated using a damage probe sample that comprises several InGaAs QW's of well widths, in order of increasing depth of 20, 40, 60, and 80 Å, separated by 200-Å InGaAsP barriers, with the uppermost (20 Å) QW situated at a depth of 300 Å, and an additional 120-Å well located approximately 4000 Å below the sample surface. The 4-K PL spectrum for the as-grown structure is shown in Fig. 2(a), and exhibits five peaks due to PL from each of the QW's. The spectrum obtained following the deposition of 200-nm sputtered SiO_2 [Fig. 2(b)] shows a marked decrease in the intensity of the narrowest wells (which are closest to the surface) and a broadening of all the peaks. However, following an anneal at 500 °C [Fig. (2(c)], the PL from all of the QW's is recovered and all the peaks exhibit a small blue shift (15 nm). These observations are consistent with the sputtering process leading to an increase in the near-surface point defect density, which reduces the PL from the QW's closest to the surface. During the anneal however, point defects will tend to diffuse both toward the sample surface and deeper into the sample, leading to a reduced defect density in the QW region and the initiation of the intermixing process through the enhanced interdiffusion of well and barrier species.

It is believed that point defects generated during the sputtered SiO_2 process can be ascribed to the bombardment by Ar ions at the sample surface, due to acceleration from the positively charged plasma to the earthed substrate electrode. This accelerating potential [10], [11] provides the ions with sufficient energy to break atomic bonds close to the sample surface, creating point defects in the form of vacancies and interstitials, and thereby enhancing the atomic interdiffusion rate. Although the generation of such point defects alone could account for the increased rate of intermixing, another possible contribution to the intermixing process could be atomic out-diffusion during the anneal stage, a mechanism similar to that responsible for the IFVD process in the GaAs–AlGaAs material. The presence of an increased concentration of point defects could lead to an enhancement in the rate of such out-diffusion and provide an additional enhancement to the intermixing rate. The possible occurrence of out-diffusion and its contributory role are the subject of ongoing investigation.

Although the long term performance of the active/passive devices fabricated using this technique, and described in the following sections, is yet to be assessed, in terms of obtaining consistent bandgap shifts this technique has proven highly reproducible and reliable for all material systems so far studied. For a given wafer annealed at the same temperature over a course of several weeks, the shifts obtained are identical to within 20%, which is due largely to variations in the calibration of the RTA. In addition, although no systematic study of the effect of surface preparation has been made, in samples that have been prepared prior to SiO_2 deposition using a range of different cleaning processes there is no apparent variation in the magnitude of the bandgap shifts obtained.

The dependence of the intermixing rate upon various sputtering parameters has been investigated in the InAlGaAs material system. Experiments have shown that the obtained bandgap shifts have very little dependence upon the RF power used during the deposition process, with variations in the self dc bias from the standard 1 kV to 300 V (with the gas pressure remaining constant at 5×10^{-3} mbar) producing exactly the same bandgap shift (103 meV) after a 3.5-h exposure to the plasma and a subsequent anneal at 700 °C. The dependence of the intermixing rate upon the gas pressure used has been investigated and shows a clear decrease in the bandgap shift for pressures below the standard pressure of 5×10^{-3} mbar (the self dc bias remaining constant at 1 kV). This observed decrease in intermixing rate may be explained simply by the reduction in the number of bombarding ions incident on the sample surface over a fixed time. At higher pressures the increasing particle density within the plasma should lead to a drop in the ion energy due to the reduction of the ion mean free path. This is expected to decrease the amount of plasma damage generated resulting in a reduced intermixing rate, although this has not been observed over the range of pressure currently studied.

Suppression of the intermixing process has been investigated using different types of capping layer to protect the sample surface during the sputtering process. Fig. 3 shows the bandgap shifts obtained in InGaAsP material following the deposition of a 200-nm sputtered SiO_2 cap and anneals at temperatures from 625 °C to 700 °C, for samples which

are unprotected, and samples which have been previously coated with either 200-nm PECVD SiO_2 or a 2-μm layer of photoresist. It is clear from this that a PECVD SiO_2 protective cap does not completely suppress the intermixing process, the capped material experiencing significant bandgap shifts (70 meV at 700 °C). This implies that, while the PECVD cap does afford some protection against the plasma damage, this is not sufficient to prevent the generation of a significant point defect density in the semiconductor and a resultant enhancement in the intermixing rate. A 2-μm protective layer of resist, however, is found to suppress the intermixing process at 650 °C completely, implying that the resist effectively absorbs the energy of the bombarding ions, preventing the formation of point defects and the associated enhancement in the intermixing rate. Similar experiments in the InAlGaAs system show that suppression can again be achieved by protecting the sample surface during the sputtering process with a previously deposited layer of either resist or SiO_2. However, unlike the InGaAsP system, bandgap shifts obtained under samples protected by PECVD SiO_2 are insignificant, suggesting that the point defect formation process is more energetic for the InAlGaAs system, as might be expected, given the greater thermal stability of this system [12]. While PECVD SiO_2 may, therefore, provide a suitable cap to suppress intermixing, layers of resist offer improved resistance to damage and a greater flexibility for subsequent device fabrication.

A number of approaches can be adopted toward obtaining a range of wavelength shifts, between zero shift and the maximum obtainable, across a single wafer, a property required for many photonic integrated circuits. One method is to use a multistage sputtering process, where the thickness of the sputtered SiO_2 layer varies across a wafer. In this case, where thinner layers are deposited the rate of intermixing at a given temperature can be significantly decreased. Alternatively, it is possible, using a single sputtering run and single anneal stage, to obtain spatial variations in wavelength shift across a wafer by using a varying thickness PECVD protective cap layer. Another more elegant approach involves the use of a technique similar to that of selected intermixing in selective areas (SISA) [8], which has proven successful in GaAs–AlGaAs with the IFVD intermixing technique. Here, by varying the filling factor of narrow intermixing suppression regions across a wafer in a single photolithography step, different bandgap shifts are obtained during an anneal, with the magnitude of the shift essentially dependent on the relative areas of intermixing enhanced regions in the specific section of the material. The investigation of these methods is currently underway.

III. Wavelength-Tuned Lasers

As the deposition of a sputtered silica film and subsequent annealing cause a substantial shift in the peak of the gain bandwidth of QW material, the technique can be utilized to fabricate lasers with a wide range of emission wavelengths on a single semiconductor wafer. Along with potential applications such as WDM communications systems and broadband detectors and sources, such devices provide an extremely useful tool for studying the effects of this intermixing process in terms of the electrical and optical quality of the processed material, with measurements of threshold current density and external slope efficiency revealing information regarding important material parameters, such as internal loss and quantum efficiency [13].

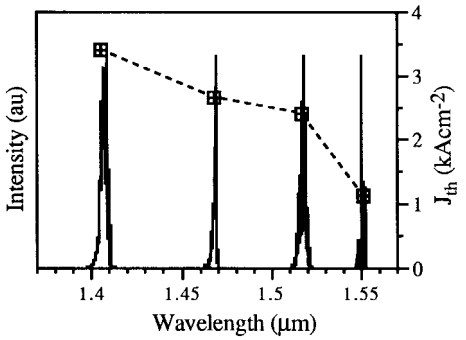

Fig. 4. Spectra of 800-μm-long InAlGaAs as-grown and wavelength tuned lasers plotted along with the increase in threshold current density $J_{\rm th}$.

To fabricate these devices, 200 nm of silica was sputtered onto four 5×5 mm^2 samples of the InAlGaAs material described in the above section. Three of these samples were annealed in an RTA at 640 °C, 665 °C, and 690 °C, respectively, for 60 s to yield PL shifts of approximately 50, 100, and 150 nm. The remaining sample was used to fabricate control devices from the as-grown material. Broad area laser stripes were fabricated by opening 75-μm windows in the SiO_2 at 300-μm intervals, using UV photolithography and wet etching. After substrate thinning and evaporation of the p-type (Ti–Pd–Au) and n-type (Au–Ge–Au–Ni–Au) metal contacts, the samples were annealed in an RTA at 360 °C for 1 min.

Devices with several different cavity lengths were cleaved from each of the four samples, and tested using a pulsed current supply with current pulses of 0.4-μs duration at 1-ms period. Fig. 4 shows the lasing spectra of typical 800-μm-long as-grown and wavelength tuned lasers, each taken at an output power of 10 mW, showing the gradual shift from the as-grown emission wavelength of 1.55–1.4 μm. Plotted along with the spectra are the corresponding laser threshold current densities. This large increase in threshold current from 1125 A·cm^{-2} in the as-grown material to 3215 A·cm^{-2} for the furthest shifted material could be ascribed to many different effects that can potentially occur during QWI processes, such as an associated diffusion of cladding layer dopants into the active region, increase in the concentration of point defects, or changes in the shape and barrier height of the QW's that cause a reduction in their two-dimensional (2-D) nature and a consequent deterioration in performance.

To investigate the probable causes of this increase, the internal quantum efficiency and internal loss of the wavelength tuned broad area lasers were estimated respectively from the y-axis intercept and gradient of an inverse external quantum efficiency against cavity length plot for each set of devices. Fig. 5 shows the calculated decrease in both loss and internal efficiency as a function of increasing bandgap shift. As demonstrated in the previous section, the intermixing process generates a large number of point defects at the sample

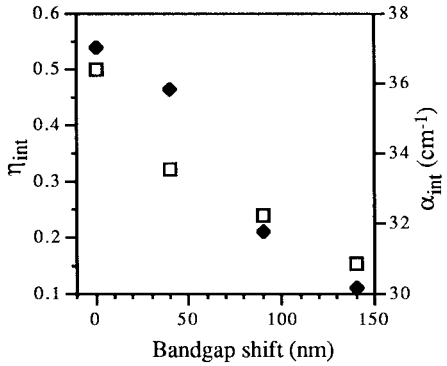

Fig. 5. Decrease in both internal quantum efficiency $\eta_{\rm int}$ (♦), and internal loss $\alpha_{\rm int}$ (□), with increasing bandgap shift for InAlGaAs wavelength tuned lasers.

surface, which subsequently diffuse and induce intermixing of the QW's. Here, this is mirrored by the large decline in the internal quantum efficiency of the wavelength tuned lasers, which may be explained by an increase in the point defect density within the active region, a consequent increase in the concentration of nonradiative recombination centres and the possible formation of extended defects. In a previous study [13] where long wavelength lasers were tuned by thermal intermixing of the quantum wells via a high power CW laser (i.e., no new point defects generated), the internal quantum efficiency remained essentially constant, with a slight increase observed in threshold current density being consistent with reduced carrier confinement in the wells. The decrease in internal loss, also noted from the plot in Fig. 5, suggests that there is no intermixing related diffusion of p-type cladding dopant (Be) into the quantum wells, which should have the opposing effect of increasing the degree of free carrier absorption in the waveguide core. A combination of the decrease in free carrier absorption in the cladding $(\propto\lambda^2)$, improved optical confinement, and a diminishing of any intraband Auger recombination are all likely to contribute toward the observed fall in internal loss as the emission is shifted to shorter wavelength.

Similar trends to the results described above have also been observed for wavelength tuned lasers fabricated using the same technique from both infrared 1.55-μm InGaAsP material and the visible GaInP–AlGaInP QW system [14], in which the lasing wavelength has been tuned from red to orange with shifts of 35 nm (equivalent to over 95 meV) being achieved from the as-grown wavelength of 676 nm.

The above results show that the sputtering induced intermixing process can be used to fabricate wavelength tuned lasers which exhibit large shifts in emission wavelength. The large increase in threshold current, in conjunction with the reduction in internal quantum efficiency, suggests that this technique would be unsuitable for active devices tuned over a wide wavelength range. Ongoing research aims to ascertain whether the observed degradation in performance can be improved upon. Ion implantation has been used to blue shift long wavelength lasers, and has shown no increase in threshold currents with shifts of over 50 nm [15]. Simmilar results with sputtered silica intermixing may potentially be achieved by significantly reducing the thickness of the sputtered film or by the use of a thin protective cap layer deposited prior to the sputtering stage. Both strategies may reduce the density of point defects introduced during the the sputtering stage. Although this is expected to reduce the observed enhancement in intermixing rate, the use of an increased anneal temperature should enable similarly large bandgap shifts to be obtained without the associated deterioration in material properties. In any case, the technique may be suitable for WDM systems where a considerably narrower range of wavelengths would be required. More importantly the observed degradation in lasing characteristics does not have any implications regarding the primary application of the technique, which is the fabrication of low-loss passive optical interconnects and monolithically integrated devices.

IV. Extended Cavity Broad-Area Lasers

In this section, the potential of the intermixing technique for the fabrication of monolithically integrated devices is demonstrated by the operation of GaInP–AlGaInP broad area extended cavity lasers. These devices comprise an oxide stripe laser integrated with passive intermixed slab waveguides on either side of the active laser section. The addition of such intermixed waveguides has been shown to lead to significant improvements in the near and far-field patterns of InGaAs–GaAs [16] lasers due to the suppression of filamentation by the diffraction of higher order transverse modes within the slab waveguides.

A similar device configuration can also be used to improve the output power from certain categories of semiconductor lasers. An important factor controlling the maximum power output of such lasers is the occurrence of catastrophic optical damage (COD). This takes place at high generated power densities, when nonradiative recombination at the facets leads to highly localized heating, resultant oxidation of the facets, and a consequent deterioration in device performance. Although such oxidation can be inhibited by coating or chemically treating the facets [17], an alternative method involves the use of nonabsorbing mirrors (NAM's) [18]–[20]. These can be easily realized using selective intermixing techniques to blue shift the absorption edge of the material in the vicinity of the facet, and thereby render the facets nonabsorbing at the lasing wavelength. NAM's have previously been demonstrated in the GaInP–AlGaInP material system [21], although a Zn impurity-induced disordering technique was used to achieve the necessary bandgap shifts.

The bandgap shifts obtained for GaInP–AlGaInP samples using the sputtered SiO_2 process are presented below, and the operation of AlGaInP extended cavity broad area lasers is demonstrated.

The GaInP–AlGaInP structures utilized were grown by MOVPE on (100) GaAs substrates misoriented by 10° toward [111] A to inhibit the occurrence of long-range ordering. The structure comprised a 500-nm Si-doped (3×10^{18} cm^{-3}) GaAs buffer layer, a 1-μm Si-doped (6×10^{17} cm^{-3}) $(Al_{0.7}Ga_{0.3})_{0.5}In_{0.5}P$ lower cladding layer, a 600 nm $(Al_{0.3}Ga_{0.7})_{0.5}In_{0.5}P$ intrinsic waveguide core, a p-type

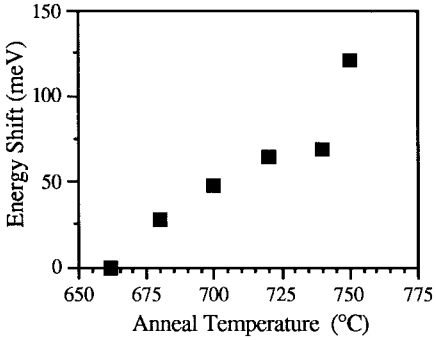

Fig. 6. Energy shift against anneal temperature for AlGaInP samples after the deposition of 200-nm sputtered SiO_2.

$(Al_{0.7}Ga_{0.3})_{0.5}In_{0.5}P$ cladding layer doped with Zn (7×10^{17} cm^{-3}), and a 0.3-μm Zn-doped (1×10^{19} cm^{-3}) GaAs cap. The active region comprised a double QW (DQW) with 2×68 Å tensile strained $Ga_{0.41}In_{0.59}P$ QW's separated by 150-Å $(Al_{0.3}Ga_{0.7})_{0.5}In_{0.5}P$ barriers centrally placed within the waveguide core.

Fig. 6 shows bandgap shifts obtained for samples capped with 200-nm sputtered SiO_2 and annealed at temperatures between 660 °C and 760 °C. Again large blue shifts are obtained, with a threshold intermixing temperature of 680 °C, and observed bandgap shifts in excess of 120 meV for an anneal temperature of 760 °C. Over the equivalent temperature range, samples capped with PECVD SiO_2 exhibited no bandgap shift.

Extended cavity oxide stripe lasers have been fabricated by first defining the intermixed and nonintermixed regions, using a 1.8-μm layer of photoresist to protect the sample surface during the sputtering process. A 200-nm layer of sputtered SiO_2 was then deposited on the sample surface using the conditions described in Section II. The resist and overlying layer of SiO_2 were then removed by liftoff in acetone and a 200-nm layer of PECVD SiO_2 deposited to protect the uncapped areas of the sample during the subsequent anneal. The sample was then annealed at 750 °C for 60 s in an RTA to produce a large differential bandgap shift between the intermixed and masked sections.

The layers of SiO_2 were removed with a wet etch and a 200-nm layer of evaporated SiO_2 deposited on the sample. Oxide stripes were then defined using photolithography and a wet etch. A wet etch was used to remove the p^+ GaAs contact layer from the passive sections to suppress current spreading from the active section. Following contact evaporation and thinning stages, the sample was annealed at 360 °C for 60 s. The sample was then cleaved to produce lasers of various lengths which were characterized using a pulsed current supply.

Fig. 7 shows the light output against injected current input (L–I) characteristics obtained for a 750-μm-long all-active laser (AAL) and an extended cavity laser (ECL) with a 750-μm-long active section, a 1000-μm-long passive section at one facet and a 500-μm-long passive section at the other. A clear increase in threshold current is observed from 470 mA for the AAL to 740 mA for the ECL (57% increase), which can largely be ascribed to diffractive losses within the intermixed passive sections.

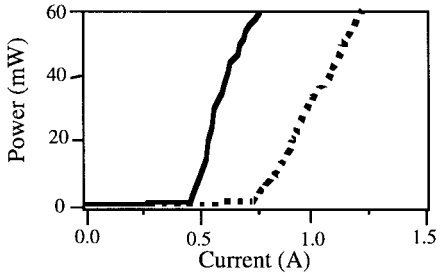

Fig. 7. L–I characteristics a 750-μm-long all active AlGaInP broad area laser (solid line), and an extended cavity laser with 750-μm-long active section and 1000/500-μm-long passive sections (dotted line).

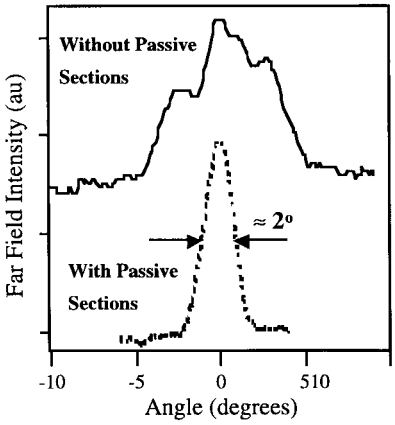

Fig. 8. Narrowing in far-field output of AlGaInP broad-area lasers with the addition of passive slab waveguide sections.

Fig. 8 shows the far-field pattern obtained for both the AAL and the ECL at twice threshold current. A marked improvement in far-field pattern was obtained from a multilobed, highly divergent pattern (with a full-width at half-maximum (FWHM) of 8°) for the AAL to a single-lobed narrow distribution (FWHM = 2°) obtained for the ECL. Such single lobed far-fields were obtained for power outputs up to 100 mW per facet. The improvement of far-field pattern from the ECL can be explained by considering the formation of filaments in an all-active broad-area laser. These filaments form due to carrier induced refractive index changes across the laser stripe and normally result in a multilobed highly divergent far-field pattern. However, with the addition of the passive slab waveguides at ends of the cavity, any filaments, which have a large diffraction angle, will experience a greater loss from diffraction in the passive slab waveguides than the fundamental Gaussian mode which is preferentially coupled back into the active section on reflection. As the filamentation is now suppressed the far-field is a consequence of the laser operating in the narrower single-lobed fundamental transverse mode.

Extended cavity broad area lasers have also been fabricated in the InAlGaAs system. In this case, the addition of slab waveguides again leads to a significant narrowing in the far-field pattern, from a multilobed pattern with FWHM = 10° for a 600-μm-long AAL, to a single-lobed pattern with FWHM = 3.5° for an ECL with a 600-μm-long active section and two 300-μm-long passive waveguides observed at output powers

up to 70 mW, with a corresponding 40% increase in threshold current from 542 to 774 mA respectively.

These results demonstrate the use of the intermixing technique for the fabrication of high-powered lasers and amplifiers with a high beam quality, with many possible applications as sources for pumping solid state lasers, e.g., Cr:LiSAF at 670 nm and Er fiber amplifiers/lasers at 1480 nm, and applications in which efficient mode-matching is required, e.g., optical time domain reflectometry. Although providing a NAM function with this intermixing technique, further lifetime testing is required to discover if any resultant reduction in facet temperture will lead to improved device lifetimes during high-power operation.

V. Extended Cavity RWG Lasers

Future photonic integrated circuits rely on the ability to produce low loss optical interconnects. The effectiveness of an intermixing technique for this purpose can be illustrated by the fabrication of extended cavity ridge waveguide (RWG) lasers. Here, intermixing enables the integration of a short active ridge waveguide of the order of 0.5 mm in length with a single long passive ridge waveguide, the absorption edge of which is blue shifted, enabling overall dimensions of several mm to be achieved. These relatively simple devices are also useful for monolithic modelocking applications when repetition rates below ~20 GHz are required [22]. In long all-active mode-locked diode lasers, optical pulses within the cavity are always present in the gain media, with the associated carrier and gain nonlinearities imparting significant effects on pulsewidth and timing jitter due to self-phase modulation. The monolithic extended cavity mode-locked laser design maintains the advantages of external cavity devices in low jitter short pulse generation, without the associated drawbacks of mechanical instability and multiple pulse formation.

To demonstrate the effectiveness of the plasma damage technique for such devices, extended cavity ridge waveguide lasers have been fabricated in the InGaAsP system. As well as thermal processing using an RTA, the effect of using a laser annealing process on the properties of the passive sections was also investigated.

A 200-nm sputtered film was deposited on two samples, one of which was annealed in an RTA to produce a differential PL shift of 110 nm using a temperature of 650 °C for 1 min, the other exposed to a CW Nd:YAG ($\lambda = 1064$ nm) laser for 3 minutes to produce a bandgap shift equivalent to that obtained in an RTA. The 77-K PL spectra of intermixed and intermixing suppressed samples after annealing are shown in Fig. 9. From the plot, the intermixed PL peak broadens from 15 to 21 meV for the laser annealed case, but only from 15 to 18.5 meV for the RTA annealing. This demonstrates that both these techniques produce material of similar optical quality, with the RTA processed material appearing to be slightly superior.

Extended cavity lasers were fabricated from samples processed using both annealing techniques to shift the bandgap of the passive section to higher energy. In both cases, the generation of point defects in the sputtering plasma was suppressed using a cap of 200-nm PECVD silica and 1.8 μm of photoresist to protect the active laser regions, while the passive sections were left uncapped. After intermixing, the samples were processed into 4-μm-wide ridge waveguides aligned along the [011] direction using a combination of CH_4/H_2 reactive ion etching and a final wet etch to remove residual surface damage. The lasers were completed by the deposition of a 200-nm PECVD silica film, the wet etching of a current injection window, substrate thinning and contact evaporation. The p-side contact was restricted only to the active section of the waveguides and, to ensure electrical isolation between the active and passive sections, the InGaAs contact layer in the passive ridge waveguide was removed by wet-etching.

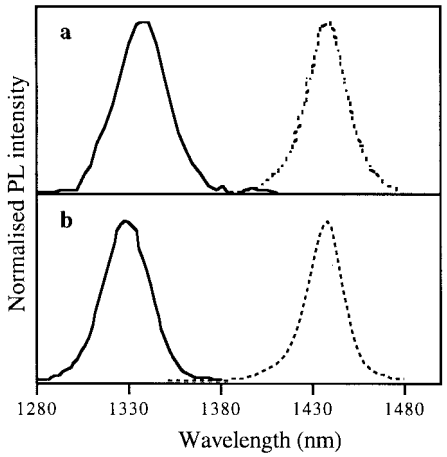

Fig. 9. Normalized PL intensity peaks for annealed (solid line) and unannealed (dotted line) InGaAsP samples with a 200-nm sputtered SiO_2 cap and annealed using (a) a CW Nd:YAG laser and (b) an RTA.

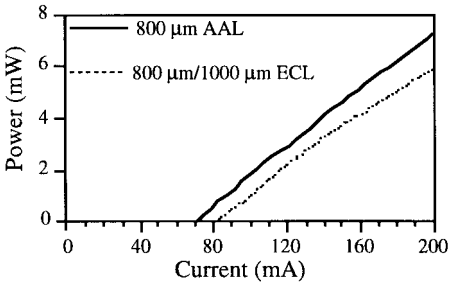

Fig. 10. L–I curves for all-active and extended cavity RWG InGaAsP lasers.

Fig. 10 shows the L–I curves for an 800-μm-long all-active RWG laser and a 1.8-mm-long ECL with 1-mm-long passive section, fabricated by the laser annealing method. Only a marginal increase in the threshold current is observed, from 73 mA for the AAL to 80 mA for the ECL. It is possible to define a relationship in QW lasers between AAL threshold current (I_{AA}), the extended cavity laser threshold current (I_{EC}), and the propagation loss in the passive section (α_p). Assuming the logarithmic gain/current density relationship for quantum wells [23] and zero reflection at the active/passive boundary [22] this relationship can be expressed as

$$\frac{I_{\mathrm{AA}}}{I_{\mathrm{EC}}} = \exp\left(\frac{\alpha_p L_p}{n\Gamma_{\mathrm{QW}} g_0 L_a}\right) \tag{1}$$

where n is the number of quantum wells, Γ_{QW} the modal overlap factor per well, g_o is the gain saturation parameter,

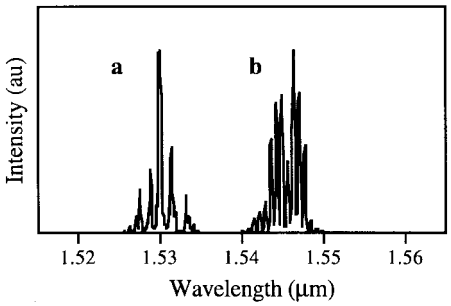

Fig. 11. Spectrum of RWG InGaAsP lasers (a) with extended cavity section and (b) with extended cavity section removed by cleaving.

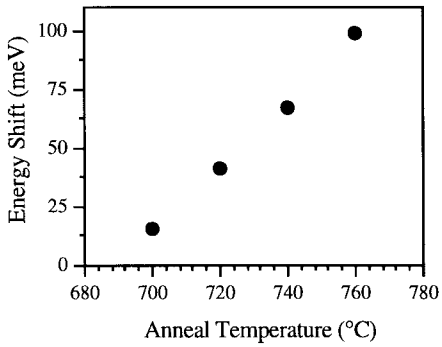

Fig. 12. Energy shifts as a function of anneal temperature for GaAs–AlGaAs MQW material capped with 200-nm sputtered SiO_2.

and L_a/L_p are the respective lengths of the active and passive laser cavities. From measurements on wide oxide stripe (75-μm) lasers, the material parameter $n\Gamma_{\rm QW}g_o$ was calculated to be 30 cm^{-1}. The estimated passive section loss is therefore $\alpha_p = 4.1$ cm^{-1}. Extended cavity lasers annealed using the conventional RTA method displayed almost identical characteristics to the above devices with the estimated passive section loss calculated to be 4.4 cm^{-1}.

With such large blue shifts of the absorpion edge compared to the lasing wavelength, and the absence of any significant dopant diffusion into the quantum wells, the passive waveguide loss is likely to be primarily due to free carrier absorption in the cladding region and is given by the following equation:

$$\alpha_f = \Gamma_{pc}\alpha_{pc} + \Gamma_{nc}\alpha_{nc} \tag{2}$$

where α_{pc} and α_{nc} represent free carrier loss in the p- and n-type waveguide cladding layers respectively. Using a finite element model to calculate the modal overlap factors in the cladding for our laser structure ($\Gamma_{pc} = \Gamma_{nc} = 0.22$) and literature values [24], [25] for the free carrier absorption coefficents at the dopant concentrations present in the InGaAsP laser structure ($\alpha_{pc} = 20$ cm^{-1} and $\alpha_{nc} = 0.5$ cm^{-1}), α_p was calculated to be 4.5 cm^{-1}, very close to the values derived experimentally. It is likely, therefore, that this value represents a fundamental lower limit to the loss achievable in the current laser structure. Optimization of the laser waveguide design by increasing width of the waveguide core to lower the modal overlap with grown-in dopants, should reduce these losses still further [26].

Interesting features are also present in the optical spectra of these lasers. AAL's fabricated from the as-grown InGaAsP material emit close to 1.55 μm in wavelength. However, as can be seen in Fig. 11, the laser spectrum from an ECL undergoes an apparent blue shift to around 1.53 μm. It is possible that a graded bandgap at the active/passive interface is responsible for this change. However, when this extended cavity is removed by cleaving, the laser emission red shifts to the original 1.55-μm wavelength. It seems likely that this effect is due to band-filling from the increase in threshold current density in the ECL, and has potentially important implications for the achievement of a required operation wavelength in integrated devices.

VI. MMI Devices

In this section, the operation of a more complex integrated device in the form of a multimode interference (MMI) coupler [27] in GaAs–AlGaAs material is demonstrated. Here, it is shown that, by using the sputtered silica QWI process, four amplifier/laser ridge waveguides can be monolithically integrated with a passive MMI coupler and passive output waveguide. This represents a new configuration for high optical power generation with a fundamental transverse mode output. Such devices are desirable for applications such as optical disk memories, free-space communications, and second-harmonic generation (SHG).

The AlGaAs structure used to study the intermixing process was a standard DQW laser structure grown by MOVPE, containing a DQW active section with 100-Å GaAs QW's separated by a 100-Å $Al_{0.2}Ga_{0.8}As$ barrier with the remaining waveguide core comprising two 0.1-μm $Al_{0.2}Ga_{0.8}As$ layers. The cladding layers comprised 0.9-μm Zn-doped p-type (5×10^{17} cm^{-3}) and 1.5-μm Si doped n-type (8×10^{17} cm^{-3}) $Al_{0.4}Ga_{0.6}As$ layers. The sample was capped by a 0.1-μm-thick p^+-Zn-doped (8×10^{18} cm^{-3}) GaAs layer.

Fig. 12 shows bandgap shifts obtained for the GaAs–AlGaAs material capped with sputtered SiO_2. The use of sputtered SiO_2 caps again leads to an increased intermixing rate, with bandgap shifts occurring initially at 700 °C and increasing in magnitude to over 100 meV at 760 °C. These large blue shifts occur at temperatures considerably lower than those normally associated with the IFVD technique (850 °C–950 °C) and, over the temperature range shown, no bandgap shifts are obtained for samples capped with PECVD SiO_2. Suppression of bandgap shifts in AlGaAs material can again be achieved using a 1.8-μm layer of resist to prevent the occurrence of sputtering induced damage.

The intermixing process was used to fabricate a 4×1 multimode interference coupler fed by four integrated RWG lasers with NAM's. The device configuration and dimensions are shown in Fig. 13. Initially, the intermixing process was used to widen the bandgap of the passive MMI, its output guide and the laser facets, using a photoresist mask to suppress intermixing in the active section. The amplifiers (4 μm wide, 2.5 μm apart), MMI, and output waveguide (4 μm wide) were then defined by dry etching to a depth 0.2 μm above the waveguide core region.

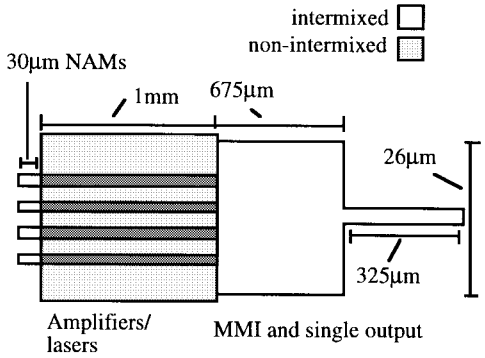

Fig. 13. Schematic diagram of the 4×1 GaAs–AlGaAs amplifier/MMI coupler.

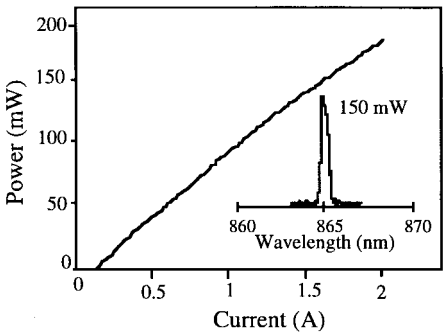

Fig. 14. L–I curve and optical spectrum of the MMI device.

Fig. 14 shows the L–I curve for the device. The threshold current was 120 mA, equivalent to 30 mA per active device. Observation of the near field during operation showed a single fundamental transverse mode output up to 180 mW, without any noticeable damage at any of the uncoated laser facets. The inset to Fig. 14 shows the optical spectrum of the laser at an injected current of 1.5 A, with the laser emission spectral width of 0.2 nm centered around 860 nm.

It is believed that the relatively low-slope efficiency of 10% per facet can be explained by the use of a single shallow etch to define the RWG's and MMI sections. This is not the best configuration for an MMI, due to the resultant poor sidewall reflectivity. Devices with deep etched MMI's and output waveguides (etched through the waveguide core) are expected to exhibit considerably improved efficiencies.

VII. Conclusion

A new intermixing technique is demonstrated, which is reliant upon the generation of point defects by plasma induced damage during the deposition of a thin layer of sputtered SiO_2. The technique appears to be universal in its application, enabling large bandgap shifts to be obtained in a number of different III–V material systems covering the wavelength range 630–1600 nm. Complete suppression of the intermixing process can easily be achieved by protecting the sample surface during the deposition process with a layer of photoresist. In addition to providing a low cost universal intermixing process, an added advantage of the technique is its extreme simplicity, enabling very large differential bandgap shifts to be obtained across a single wafer in a single, straightforward, lithography step.

The potential applications of the technique are demonstrated through the fabrication and characterization of a number of active and passive/integrated devices. The operation of wavelength tuned lasers has been studied over the ranges 630–660 nm and 1400–1550 nm, and has shown that the large point defect density required to produce substantial bandgap shifts causes significant degradation in the internal quantum efficiency of devices, but does not seriously affect the internal loss. This was further illustrated by the successful operation of extended cavity broad-area lasers in AlGaInP and InAlGaAs: narrow single-lobed far-field patterns were obtained at wavelengths of 650 and 1550 nm, respectively. Extended cavity ridge waveguide lasers, fabricated in the InGaAsP system, demonstrated low passive waveguide losses of ~ 4 cm^{-1} at an emission wavelength close to 1550 nm. Calculations have shown that this value is essentially limited by free carrier absorption loss in the laser waveguide cladding layers and further optimization of the structure should enable lower losses to be readily attained. Finally, a sophisticated integrated device in the AlGaAs MQW system has been demonstrated using this intermixing technique, to provide both a nonabsorbing mirror function and a passive MMI section to couple the output of four laser amplifier sections together. The production of high output powers (>150 mW) at 860 nm in a single transverse mode output beam was demonstrated.

To summarize, these results illustrate that the technique provides a simple, low cost and reliable intermixing process for a variety of different III–V material systems, and should therefore enable significant and rapid advances in the routine fabrication of photonic integrated circuits.

Acknowledgment

The authors gratefully acknowledge the assistance of J. Young and I. McNichol in the maintenence and operation of the sputtering equipment, and to Dr. S. Hicks for helpful discussions.

References

[1] W. D. Laidig, N. Holonyak, Jr., M. D. Camras, K. Hess, J. J. Coleman, P. D. Dapkus, and J. Bardeen, "Disorder of an AlAs-GaAs superlattice by impurity diffusion," *Appl. Phys. Lett.*, vol. 38, pp. 776–778, 1981.

[2] L. J. Guido, N. Holonyak Jr., K. C. Hseih, R. W. Kaliski, W. E. Plano, R. D. Burnham, R. L. Thornton, J. E. Epler, and T. L. Paoli, "Effect of dielectric encapsulation and As overpressure on Al-Ga interdiffusion in $Al_xGa_{1-x}As$ quantum well heterostructures," *J. Appl. Phys.*, vol. 55, pp. 540–542, 1989.

[3] J. E. Epler, F. A. Ponce, F. K. J. Endicott, and T. L. Paoli, "Laser disordering of GaAs/AlGaAs by diffusion of laser incorporated Si," *J. Appl. Phys.*, vol. 64, pp. 3439–3444, 1988.

[4] C. J. McLean, J. H. Marsh, R. M. De La Rue, A. C. Bryce, B. Garrett, and R. Glew, "Layer selective disordering by photo-absorption induced thermal diffusion in InGaAs/InP based multiple quantum well structures," *Electron. Lett.*, vol. 28, pp. 1117–1119, 1992.

[5] A. McKee, C. J. McLean, G. Lullo, A. C. Bryce, R. M. De La Rue, J. H. Marsh, and C. C. Button, "Monolithic integration in InGaAs-InGaAsP multiple-quantum-well structures using laser intermixing," *IEEE J. Quantum Electron.*, vol. 33 pp. 45–55, 1997.

[6] B. Tell, J. Shah, P. M. Thomas, J. W. Sulhoff, K. F. Brown-Goebler, A. D. Giovanni, B. I. Miller, and U. Koren, "Phosphorous ion implantation

induced intermixing of InGaAs/InP quantum well structures," *Appl. Phys. Lett.*, vol. 54, pp. 1570–1572, 1989.
[7] D. G. Deppe and N. Holonyak Jr., "Atom diffusion and impurity-induced layer disordering in quantum well III–V semiconductor heterostructures," *J. Appl. Phys.*, vol. 64, pp. 93–113, 1988.
[8] B. S. Ooi, K. McIlvaney, M. W. Street, A. S. Helmy, S. G. Ayling, A. C. Bryce, J. H. Marsh, and J. S. Roberts, "Selective quantum well intermixing in GaAs-AlGaAs structures using impurity free vacancy diffusion," *IEEE J. Quanum Electron.*, vol. 33, pp. 1784–1793, 1997.
[9] P. Cusamano, J. H. Marsh, M. J. Rose, and J. S. Roberts, "High-quality extended cavity ridge lasers fabricated by impurity free vacancy diffusion with a novel masking technique," *IEEE Photon. Technol. Lett.*, vol. 9, pp. 282–284, 1997.
[10] J. V. Scanlan and M. B. Hopkins, "Langmuir probe measurements of the electron energy distribution in radio-frequency plasmas," *J. Vac. Sci. Tehcnol. A*, vol. 10, pp. 1207–1211, 1991.
[11] S. Maniv, "Modeling for rf discharge characteristics," *J. Appl. Phys.*, vol. 63, pp. 1022–1031, 1988.
[12] A. C. Bryce, J. H. Marsh, R. Gwilliam, and R. W. Glew, "Impurity induced disordering in InGaAs/InGaAlAs quantum well using implanted flourine and boron," *Proc. Inst. Elect. Eng.-J.*, vol. 138, pp. 87–90, 1991.
[13] A. McKee, C. J. McLean, A. C. Bryce, R. M. De La Rue, J. H. Marsh, and C. Button, "High quality wavelength tuned muliquantum well GaInAs/GaInAsP lasers fabricated using photoabsorption induced disordering," *Appl. Phys. Lett.*, vol. 65, pp. 2263–2265, 1994.
[14] C. J. Hamilton, O. P. Kowalski, K. McIlvaney, and J. H. Marsh, "Band gap shifted visible laser diodes," in *Proc. IEEE LEOS'97*, San Francisco, CA, 1997, paper ThT4.
[15] S. Charbonneau, P. J. Poole, Y. Feng, G. C. Aers, M. Dion, M. Davies, R. D. Goldberg, and I. V. Mitchell, "Band-gap tuning of InGaAs/InGaAsP/InP laser using high energy ion implantation," *Appl. Phys. Lett.*, vol. 67, pp. 2954–2956, 1995.
[16] K. McIlvaney, J. Carson, A. C. Bryce, J. H. Marsh, and R. Nicklin, "Far-field behavior of 980 nm broad area lasers incorporating bandgap widened extended slab waveguides," *Electron. Lett.*, vol. 31, pp. 533–544, 1995.
[17] N. K. Dutta, W. S. Hobson, G. J. Zydzik, J. F. de Jong, P. Parayanthal, M. Passlack, and U. K. Chakrabarti, "Mirror passivation of InGaAs lasers," *Electron. Lett.*, vol. 33, pp. 213–214, 1997.
[18] H. Naito, M. Kume, K. Hamada, H. Shimizu, and G. Kano, "Highly-reliable CW operation of 100 mW GaAlAs buried twin ridge substrate lasers with nonabsorbing mirrors," *IEEE J. Quantum Electron.*, vol. 25, pp. 1495–1499, 1989.
[19] M. Matsumoto, K. Sasaki, M. Kondo, T. Ishizumi, T. Takeoka, H. Nakatsu, M. Watanabe, O. Yamamoto, and S. Yamamoto, "High-power 780 nm AlGaAs narrow-stripe window structure lasers with window grown on facets," *Jpn. J. Appl. Phys.*, vol. 32, pp. 665–667, 1993.
[20] P. G. Piva, S. Fafard, M. Dion, M. Buchanan, S. Charbonneau, R. D. Goldberg, and I. V. Mitchell, "Reduction of InGaAs/GaAs laser facet temperatures by band gap shifted extended cavities," *Appl. Phys. Lett.*, vol. 70, pp. 1662–1664, 1997.
[21] A. Shima, H. Tada, T. Motoda, M. Tsugami, T. Utakouji, and H. Higuchi, "Reliability study on 50–100-mW CW operation of 680-nm visible laser diodes with window-mirror structure," *IEEE J. Select. Topics Quantum Electron.*, vol. 3, pp. 443–449, 1997.
[22] F. Camacho, E. A. Avrutin, P. Cusumano, A. S. Helmy, A. C. Bryce, and J. H. Marsh, "Improvements in mode-locked semiconductor diode lasers using monolithically integrated passive waveguides made by quantum-well intermixing," *IEEE Photon. Technol. Lett.*, vol. 9, pp. 1208–1210, 1997.
[23] P. W. A. McIlroy, A. Kurobe, and Y. Uematsu, "Analysis and application of theoretical gain curves to the design of multiquantum well lasers," *IEEE J. Quantum Electron.*, vol. 21, pp. 1958–1963, 1985.
[24] W. Dumke, M. Lorenz, and G. Pettit, "Intra- and interband free-carrier absorption and the fundamental absorption edge in n-type InP," *Phys. Rev. B*, vol. 1, pp. 4668–4673, 1970.
[25] A. Ballman, A. Glass, R. Nahory, and H. Brown, "Double doped low etch pit density InP with reduced optical absorption," *J. Cryst. Growth*, vol. 62, pp. 198–202, 1982.
[26] D. Garbuzov, L. Xu, S. R. Forrest, R. Menna, R. Martinelli, and J. C. Connolly, "1.5 μm wavelength, SCH-MQW InGaAsP/InP broadened-waveguide laser diodes with low internal loss and high output power," *Electron. Lett.*, vol. 32, pp. 1717–1719, 1996.
[27] L. B. Soldano and E. C. M. Pennings, "Optical multi-mode interference based on self imaging: Principles and applications," *J. Lightwave Technol.*, vol. 13, pp. 615–627, 1995.

Stewart D. McDougall was born in Scotland, U.K., in 1972. He received the first class B.Eng. (honors) degree in physics and electronic engineering in 1993 and the Ph.D. degree in optoelectronics in 1997, both from the University of Glasgow, Glasgow, Scotland, U.K. His Ph.D. research involved work on high-repetition mode-locking of quantum-well semiconductor lasers and was a CASE studentship with BT Laboratories Martelsham Heath, U.K.

He is currently employed as a Research Assistant in the Optoelectronics Research Group of the Department of Electronics and Electrical Engineering at the University of Glasgow, where he is involved in the development of long-wavelength mode-locked semiconductor lasers, quantum-well intermixing techniques, and high-speed photodetectors.

Olek P. Kowalski was born in Montreal, Canada. He receieved the B.Sc. and Ph.D. degrees in physics from the University of Sheffield, Sheffiled, U.K., in 1992 and 1996, respectively. His Ph.D. research involved an optical spectroscopic study of the band structure of bulk AlGaInP and related quantum-well structures, in collaboration with Sharp Laboratories of Europe and lead to a significantly improved knowledge of many of the material parameters and a direct observation of long-range crystal ordering in AlGaInP.

Since March 1996, he has been employed as a Research Assistant at the University of Glasgow where has been working on optoelectronic device integration using quantum-well intermixing techniques, mode-locked lasers and OTDM systems.

Craig Hamilton was born in 1970 in Paisley, Scotland, U.K. He received the B.Eng. degree in electrical and electronic engineering in 1992 from the University of Paisley, and the Ph.D. degree in 1995.

While performing undergraduate work, he also worked for W. L. Gore and the Admiralty. He was awarded the J. D. Gray scholarship from the University of Glasgow to pursue research in nonlinear optics and observing solitonic effects in semiconductor ARROW structures. He is currently employed at the university where his research interests include integrated nonlinear optic devices, and optical integration within novel visible semiconductor laser arrays.

Fernando Camacho, photograph and biography not available at the time of publication.

Bocang Qiu was born in Shaanxi, China, in 1962. He received the B.Eng. degree in the electronic engineering from Xi'an Jiaotong University, Xi'an, China, in 1983, the M.Eng. degree from Beijing Institute of Technology, Beijing, China, in 1996, and the Ph.D. degree in the Department of Electronics & Electrical Engineering, from University of Glasgow, Glasgow, Scotland, U.K., in 1998.

Subsequently, he was appointed to an academic position in Xi'an Jiaotong University and worked in electron beam, ion beam and microfabrication technology. His research was concerned with the photonic integration in InGaAs–InGaAsP material system using quantum well intermixing. Currently, he is a post-doctoral Research Assistant in the same department, working on photonic integrated gigabit switches for 100-Gb/s packet communication.

Maolong Ke, photograph and biography not available at the time of publication.

Richard M. De La Rue (M'94–SM'96) was born in Reading, U.K., in 1945. He received the B.Sc.(Eng.) (honors) degree in electrical engineering from University College London (UCL), London, U.K., in 1966, the M.A.Sc. degree in electrical engineering at the University of Toronto, Toronto, ON, Canada, in 1968 and the Ph.D. degree, also from UCL, in 1972.

In 1971, he was appointed as Lecturer in the Department of Electronics and Electrical Engineering at the University of Glasgow, becoming Senior Lecturer in 1982, Reader in 1985, and Professor of Optoelectronics in 1986. He spent a six-month period at Bell Laboratories, Murray Hill, NJ, in 1978, and three months as a Monbusho/British Council sponsored lecturer at Tohoku University, Sendai, Japan, in 1980. A paper based on the Ph.D. work received the premium for the best paper published in *Proceedings of the Institution of Electrical Engineers* in 1972. He has contributed significantly to integrated optics research in glass-based waveguides, including the use of ion-exchange techniques. Such waveguides have been used in more recent research on optical waveguide molecular sensors. Work on lithium niobate led to the first publications in the U.K. on waveguide devices (both electrooptic and acoustooptic) and some of the earliest waveguide devices in the world based on proton-exchange in lithium niobate. He was involved in pioneering work on electron beam induced domain reversal to produce periodic structures for quasiphase matched SHG. Other work has included fundamental studies of the proton-exchange process in lithium niobate and lithium tantalate. Recent work has been concerned primarily with integration technology and optoelectronic devices based on III–V semiconductor quantum-well heterostructures. Research has included quantum well intermixing processes in III–V semiconductors to shift the refractive index and absorption edge—and novel forms of DFB and DBR laser using deep surface gratings. He has also contributed to the development of ring geometry semiconductor lasers—particularly large diameter mode-locked devices. Following an extended period as leader of the SERC/EPSRC Rolling Grant supported optoelectronics research activity at Glasgow University, he has now shifted a significant part of his research effort into the photonic bandgap structures/microcavities area. He has published more than 160 articles and papers in journals, book chapters and conference presentations. He was co-editor, with J. Marsh, of *Waveguide Optoelectronics*, based on the 1990 NATO ASI held in Glasgow, Scotland, U.K.

Dr. De La Rue is a member of Institution of Electrical Engineers and the Optical Society of America, and was elected a Fellow of the Royal Society of Edinburgh in 1989.

A. Catrina Bryce (M'91) was born in Galsgow, Scotland, U.K., in 1956. She received the B.Sc. degree in physics from Glasgow University, Glasgow, Scotland, U.K., in 1978, the M.Sc. degree in amorphous materials from Dundee University, Scotland, U.K., in 1979, and the Ph.D. degree in phonon scattering in thin-film glasses from Glasgow University.

She joined the Department of Electronics and electrical Engineering, University of Glasgow, in 1985, as a Research Assistant in molecular beam epitaxy. In 1987, she joined the optoelectronics group to work on nonlinear optical properties of GaInAs quantum-well structures at 1.5 μm. Since then, her research work has included GaInAs–InP electrooptic modulator, quantum-well intermixing particularly in 1.55 μm and 980-nm material systems, and lasers at both 980 nm and 1.55 μm. Her main research interests are optoelectronic integration and short-pulse semiconductor lasers.

John H. Marsh (M'91–SM'91), for photograph and biography, see this issue, p. 583.